31st Congress of the International Council of the Aeronautical Sciences
Belo Horizonte, Brazil; September 09-14, 2018

AERODYNAMIC DESIGN OF KEY COMPONENTS OF THE LARGE-DISCHARGE AXIAL FAN AT HIGH ALTITUDE

XuDong Yang, ZhongBao Liu, ShunLei Zhang, Chao Song
School of Aeronautics, Northwestern Polytechnical University, Xi'an, China

Keywords: *airship; axial fan; low Reynolds number; CFD*

Abstract

The large-discharge axial fan is the key equipment of stratospheric airship. Compared with the common fan, the large-discharge fan at high altitude works at the low-Reynolds-number conditions. Its performance plays an important role on the airship energy system and lift control system. Based on the computational fluid dynamics (CFD) method, this paper studies the flow field characteristics of the large-discharge fan and the effect of the blade cross section airfoils firstly. Then the influence of key components, including the current collector, the diffuser, and the front guide vane, is researched deeply. Results show that the fan with high lift-drag ratio low-Reynolds-number airfoil, streamline current collector, cylindrical wind tube, streamline tail cone and suitable number of front guide vanes is the best choice for the large-discharge fan at high altitude.

1 Introduction

Recently, near-space long-endurance airship, which can stay for a long time at high altitude and be reusable, is given more and more attention. Especially, the high-altitude large-discharge axial fan is always equipped to inflate and deflate gasbags to keep the shape of the airship and control the airship for lifting up and down. But because of the low density at the high altitude, the buoyancy of the near-space airship is small and the axial fan works at the low-Reynolds-number conditions. The performance of the large-discharge axial fan is essential to the lift control system of the near-space airship.

Especially, the low-Reynolds-number effect of the fan blade cross section airfoil becomes remarkable as the airship works above 20km, which affects the aerodynamic characteristics of the airfoil and the whole performance of the fan. However, most fan blade cross section airfoils, for example NACA airfoils, CLARK Y airfoil, LS airfoil and circular-arc airfoil, are designed for the high-Reynolds-number conditions. At the low-Reynolds-number conditions, the laminar separation will appear on the airfoil because of the difficulty to overcome the adverse pressure gradient and also the laminar separation bubbles (LSBs) will exist. For the common high-Reynolds-number airfoils, the LSBs appear at the small angles of attack (AoAs), which causes that the lift coefficient of the airfoil is small and the drag coefficient increases extremely. Therefore, it is necessary to apply the low-Reynolds-number airfoil to the high-altitude large-discharge fan. Lots of studies on the low-Reynolds-number airfoils and phenomenon were made by many researchers [1-6].

Also, forefathers made much effort on the fan design. Benini [7] developed a method for transonic compressor multi-objective design optimization and applied to the NASA rotor 37. The optimal rotor configurations with larger maximum pressure ratio and maximum efficiency were obtained. Vad [8] investigated the effects of circumferential forward skew on fan blade aerodynamics and carried out comparative studies on two axial flow fan rotors of controlled vortex design at their design flow rate. Seo [9] performed numerical optimization for design of blade stacking line for an axial flow fan with response surface method. Louw [10]

presented a design methodology for single-rotor axial flow fans, appropriate for use in large industrial air-cooled heat exchangers. However, less research on the key components of the high-altitude large-discharge axial fan were made.

Therefore, in this paper, the flow-field characteristics of the large-discharge axial fan working at 20km are studied. The influence of the large-discharge axial fan key components, including airfoils, current collector, diffuser and front guide vane, are researched deeply.

2 Numerical Setup

2.1 Numerical Methods

The CFD method based on the Reynolds-Averaged Navier-Stokes equations (RANS) is implemented in this paper and the $k-\omega$ SST turbulence coupled with the $\gamma-Re_\theta$ transition model [11,12] is used. In addition, the finite-volume method with second-order spatial accuracy is used to solve the governing equations whilst the second-order accurate, implicit time-integration and "Frozen Rotor" approach are utilized.

2.2 Grid Convergence Analysis

The geometric parameters of the computed fan are as follows: hub ratio, 0.56; external diameter, 200mm; blade number, 10; tip clearance, 1mm. As shown in Fig.1, it is a single-stage fan with the front guide vanes, current collector, tail cone, fairing, etc.

The multi-block structured grid, including rotary domain and stationary domain, is employed. The rotary components of the fan, for example, blades and hub, are included in the rotary domain to simulate the rotating effect. Meanwhile, the far-field boundaries, front guide vanes, current collector and diffuser are included in the stationary domain. The fluid-field information transmissions are through the interface between the rotary domain and stationary domain.

To validate the grid convergence, three different size grids are generated: a coarse grid with 2.5 million cells, a medium grid with 6.0 million cells and a fine grid with 12.0 million cells. The simulation conditions are set using the atmospheric parameters at 20km. Fig.2 shows the surface grid of the hub, front guide vanes and fan blades when the overall grid number is 6.0 million. Fig.3 and Fig.4 show the influence of the grid number to the total pressure and efficiency. The computed total pressure and efficiency at the coarse grid are underestimated at each air flow rate compared to results at the medium gird and fine grid. But the computed total pressure and efficiency at the medium grid are basically identical with the results at the fine grid. Considering the computational complexity and accuracy, the medium grid is further used to study the influence of the key components of the fan.

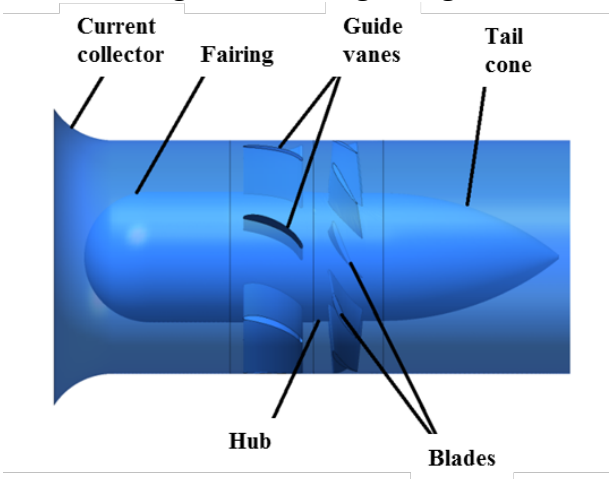

Fig.1 Schematic of the large-discharge fan

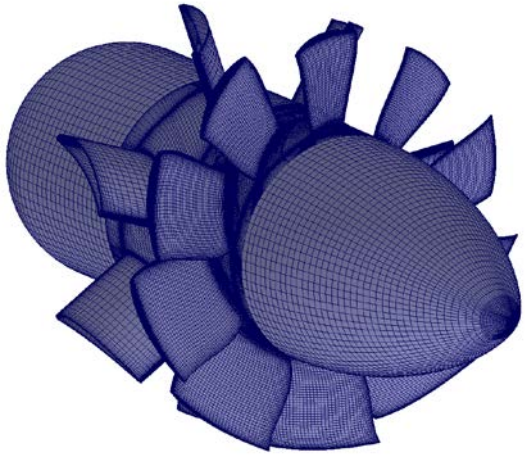

Fig.2 Surface grid of the axial fan (medium grid)

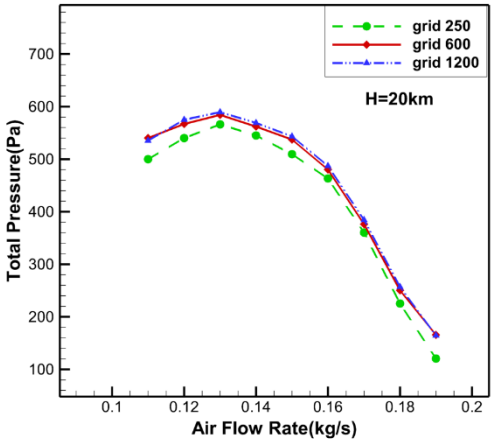

Fig.3 Total pressure versus air flow rate at different grid numbers

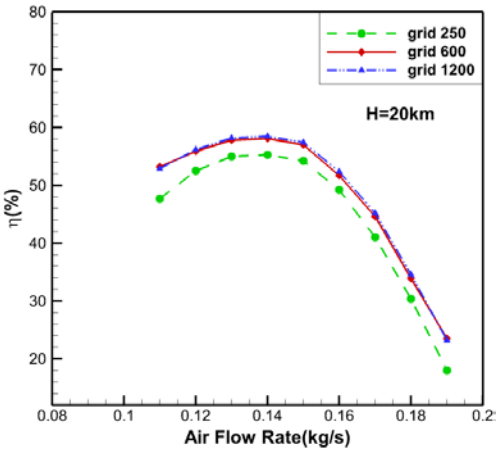

Fig.4 Efficiency versus air flow rate at different grid numbers

3 Results and Discussions

3.1 Flow-Field Characteristics at 20km

This section provides in-depth analysis about the flow-field characteristics of the large-discharge fan at the maximum air flow rate condition, based on the results at the medium grid in section 2.2. As shown in Fig.3, the maximum air flow rate of this large-discharge fan is 0.19kg/s. Fig.5 and Fig.6 show the pressure contours of the fan blade leeward and windward surfaces when the air flow rate is 0.19kg/s. There is a large pressure gradient on the windward surface of the fan blade, and almost all the middle regions of the windward surface are the low-pressure regions. Also, the area of the high-pressure region at the leading edge is larger than that at 0km.

Fig.7 shows the surface streamlines of the fan blade and Fig.8 shows the streamlines and pressure contours of the fan blade cross section airfoils in sections r/R=0.1, r/R=0.4 and r/R=0.8, respectively. The pressure distributions of these three profiles are similar, and the high-pressure regions at the leading edge become bigger and bigger as the radius of blade sections increase. There are distinct flow separations at the root of the fan blade. But no obvious separation exists in the 40% fan blade cross section, indicating that the separation exists only near the hub. The possible reason of this phenomenon is that there is transverse pressure gradient between adjacent blades.

Fig.9, Fig.10 and Fig.11 show the spatial streamlines and vorticity contours of the fan. It is shown that the velocity field is uniform before the fan inlet and the rotational effect caused by the fan blades makes the total pressure loss at the fan outlet.

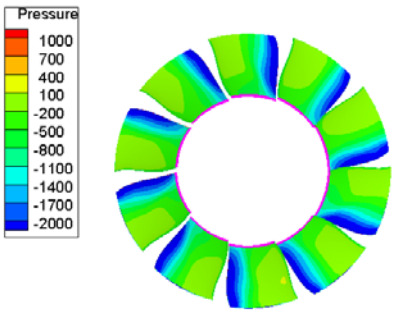

Fig.5 Pressure contours of the fan blade leeward surfaces

($\dot{m} = 0.19kg/s$)

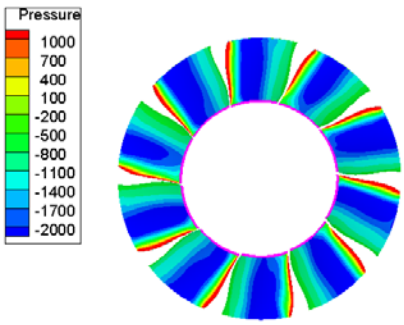

Fig.6 Pressure contours of the fan blade windward surfaces

($\dot{m} = 0.19kg/s$)

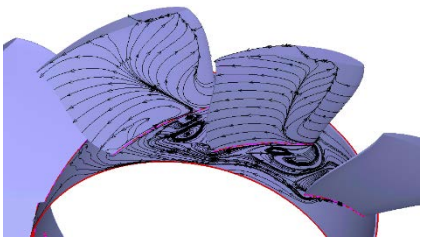

Fig.7 Surface streamlines of the fan blade ($\dot{m} = 0.19kg/s$)

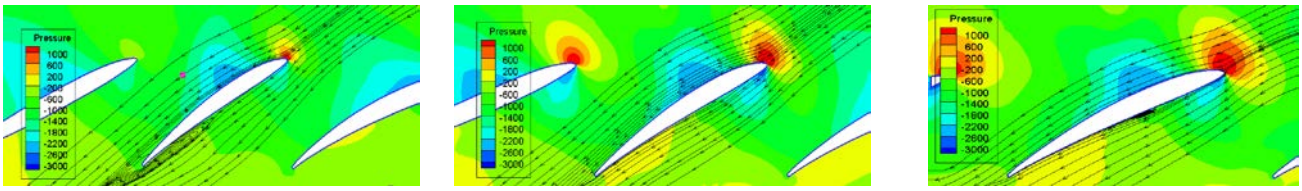

(a) r/R=0.1 **(b) r/R=0.4** **(c) r/R=0.8**

Fig.8 Streamlines and pressure contours of the fan blade cross section airfoils ($\dot{m} = 0.19kg/s$)

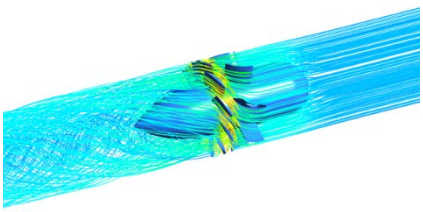

Fig.9 Spatial streamlines of the fan ($\dot{m} = 0.19kg/s$)

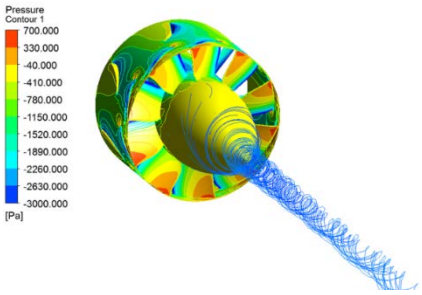

Fig.10 Spatial streamlines induced by the hub ($\dot{m} = 0.19kg/s$)

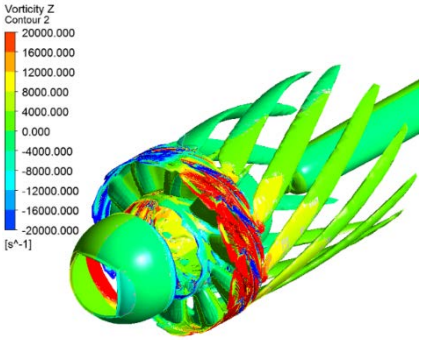

Fig.11 Vorticity contours of the fan ($\dot{m} = 0.19kg/s$)

3.2 Influence of Airfoils

The fan blade cross section airfoil plays a crucial role in the performance of the fan. In order to significantly improve the overall performance of the fan at high altitude, the airfoil with high lift-drag ratio at low-Reynolds-number conditions is required.

This section first analyzes the performance of the commonly used CLARK Y airfoil and the self-designed low-Reynolds-number PLRMS10 airfoil at 5×10^4 Reynolds number. As shown in Fig.12, the C-type grid is employed. The computational domain extends from 25 chords upstream of the leading edge to 30 chords downstream of the tailing edge and 25 chords above and below the airfoil. The first layer spacing meets $y^+<1$. Fig.13, Fig.14 and Fig.15 show the aerodynamic characteristics of these two airfoils. At the same AoA, the lift coefficient of PLRMS10 airfoil is larger than that of CLARK Y airfoil while the drag coefficient of PLRMS10 airfoil is smaller than that of CLARK Y airfoil. Meanwhile, the stall AoA of PLRMS10 airfoil is 10 deg and CLARK Y airfoil stalls at 8 deg. Therefore, the aerodynamic characteristics of PLRMS10 airfoil is significantly better than that of CLARK Y airfoil at 5×10^4 Reynolds number.

Then, the overall performance of fans using the above two airfoils and the flat airfoil are analyzed when the other geometric parameters of fans are unchanged. Fig.16 and Fig.17 respectively show the total pressure and efficiency of fans using different airfoils. Results show that at the same air flow rate, the total pressure and efficiency of the fan using PLRMS10 airfoil are higher than that of fans using the other two airfoils. Taking the air flow rate of 0.15kg/s as an example, the total pressure of the fan using PLRMS10 airfoil is about 9% and 25% higher than that of fans using CLARK Y airfoil and flat airfoil, respectively. The efficiencies are improved by about 10% and 24%. Also, the fan using flat airfoil has a maximum efficiency of only about 50%. The maximum total pressure of the fan using flat airfoil is 100Pa less than that of the fan using PLRMS10 airfoil.

Therefore, the PLRMS10 airfoil with high lift-drag ratio at low-Reynolds-number condition is selected as the blade cross section airfoil, which helps to increase the total pressure and efficiency, reduce the flow losses and increase the maximum air flow rate of the fan.

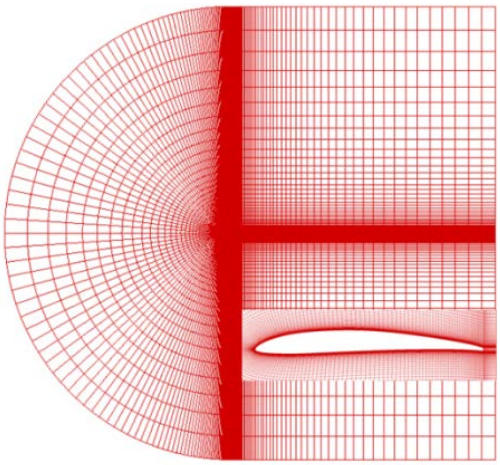

Fig.12 C-type grid for PLRMS10 airfoil

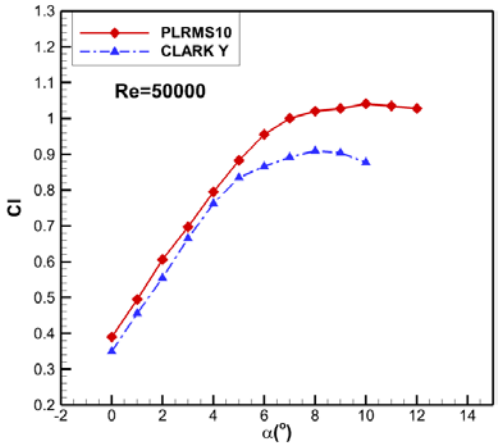

Fig.13 Comparison of lift coefficients for different airfoils ($Re=5\times10^4$)

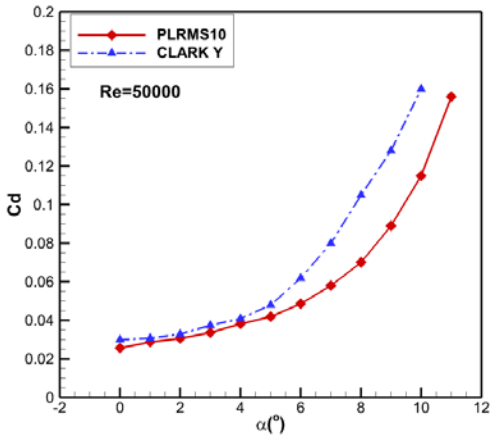

Fig.14 Comparison of drag coefficients for different airfoils ($Re=5\times10^4$)

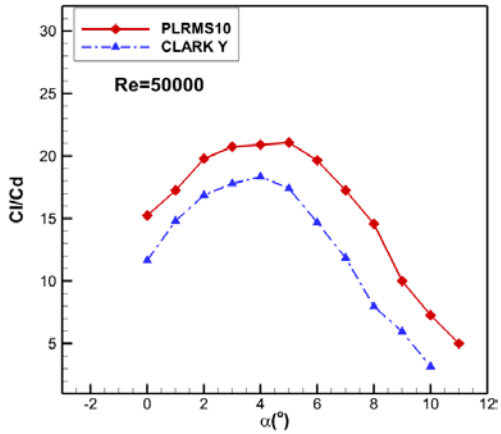

Fig.15 Comparison of lift-drag ratios for different airfoils ($Re=5\times10^4$)

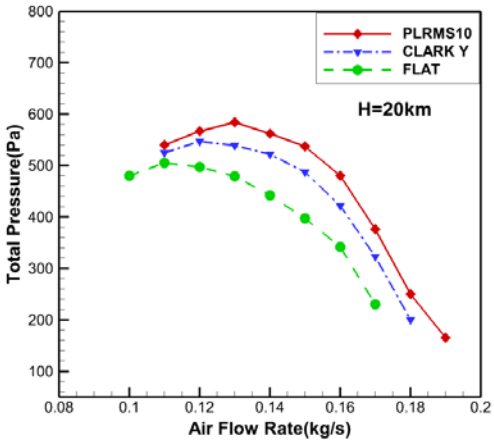

Fig.16 Total pressure versus air flow rate for fans using different airfoils

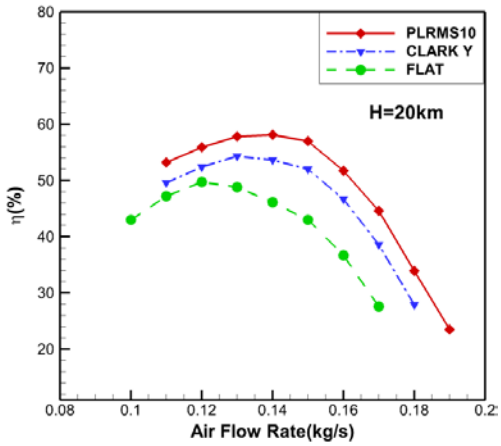

Fig.17 Efficiency versus air flow rate for fans using different airfoils

3.3 Influence of Current Collectors

A current collector is usually installed at the front of the fan in order to accelerate the gas in the tapered duct and establish a uniform flow field. This section studies the influence of different types of current collectors to the performance of the large-discharge fan. As shown in Fig.18 and Fig.19, the three current collectors are the straight-tube type current collector, the arc-type current collector, and the streamline current collector.

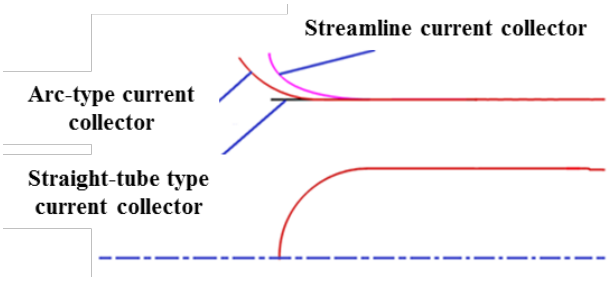

Fig.18 Sectional views of three current collectors

Table 1 shows the maximum air flow rate and power of the fans at the ideal inlet conditions and using the three different current collectors. Results show that compared with results of the fan at the ideal inlet conditions, the maximum air flow rate of the fan using the straight-tube type current collector is significantly reduced by about 400 m^3/h, and its power is also higher than that of fans using the other current collectors. Also, the maximum air flow rate of the fan using the arc-type current collector is reduced by approximately 1.36% and the power is increased by approximately 2.9%. Especially for the fan using streamline current collector, its maximum air flow rate is only about 0.7% lower than that of the fan at the ideal inlet conditions, and its power is only increased by about 15.3W. Therefore, the streamline current collector is a better choice to improve the overall aerodynamic performance of the fan at high altitude.

Table 1 Influence of the current collectors on the maximum air flow rate of the fans (H=20km)

Types of Current Collectors	Maximum Air flow rate (m^3/h)	Power (W)
Ideal inlet conditions	7744.3	1500.3
Straight-tube type current collector	7340.8	1572.4
Arc-type current collector	7640.7	1542.4
Streamline current collector	7690.9	1515.3

Fig.20 shows streamlines of three current collectors at the maximum air flow rate conditions. It is shown that the large flow separation region appears at the inlet lip of the straight-tube type current collector and the inlet flow uniformity is poor, leading to an increase in the flow loss. The arc-type current collector significantly weakens the flow separation. The inlet flow is relatively uniform, and the flow loss is relatively small. The flow separation at the inlet lip of the streamline current collector is further weakened and the flow loss is minimized.

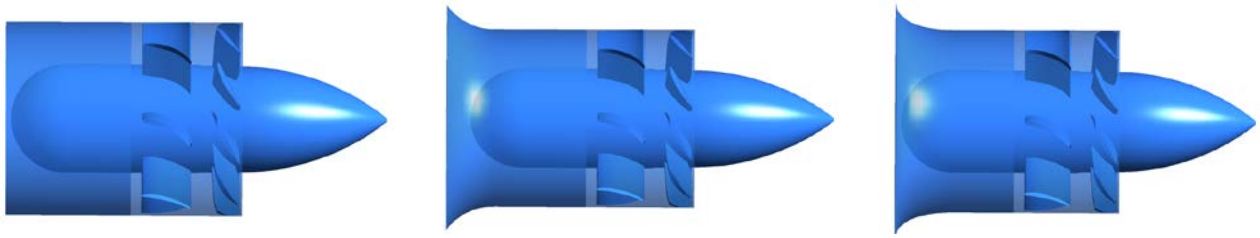

(a) Straight-tube type current collector **(b) Arc-type current collector** **(c) Streamline current collector**

Fig.19 Schematics of fans using different current collectors

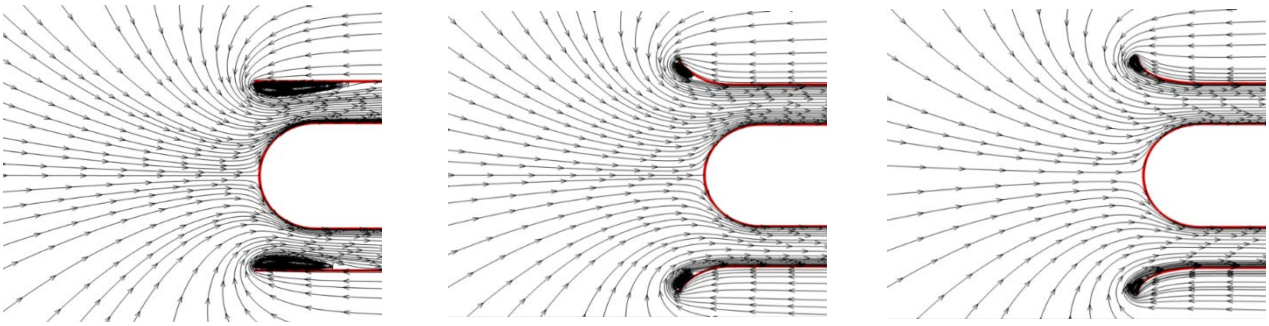

(a) Straight-tube type current collector (b) Arc-type current collector (c) Streamline current collector

Fig.20 Streamlines of fans using different current collectors at maximum air flow rate conditions

3.4 Influence of Diffusers

In order to increase the static pressure and reduce the axial velocity of the fan outlet, the diffuser becomes one of the indispensable key components of the fan. This section researches several different diffusers, as shown in Fig.21. Type 1, Type 2 and Type 3 diffusers use the cylindrical wind tube. Type 4 diffuser uses the conical wind tube. There is no tail cone in Type 1 diffuser, the streamline tail cone in Type 2 diffuser, the extended tapered tail cone in Type 3 diffuser and the cylindrical tail cone in Type 4 diffuser.

Table 2 shows the numerical results of the total pressure and efficiency of the fans using different diffusers at air flow rate of 0.14 kg/s and 0.18 kg/s, respectively. It is shown that when the air flow rate is 0.14kg/s, the total pressures of fans using Type 2, Type 3 and Type 4 diffusers are increased by about 15%, 18.4%, and 13.4%, respectively, compared to that of fan using Type 1 diffuser, and the efficiencies are increased by about 17.8%, 21.5% and 18.3%, respectively. When the air flow rate is 0.18kg/s, the total pressures of fans using Type 2, Type 3 and Type 4 diffusers are increased by about 87%, 116.7%, and 85.2%, respectively, compared to that of fan using Type 1 diffuser, and the efficiencies are increased by about 108%, 127.6% and 103.1%, respectively. The total pressure and efficiency of fan using Type 3 diffuser are the largest. Because of no tail cone in Type 1diffuser, fan's total pressure and efficiency are the lowest. Therefore, the tail cone can increase the total pressure and efficiency of the fan at high altitude, especially for the large-discharge fan.

Table 2 Influence of the diffusers on the performance of the fans (H=20km)

Types of Diffusers	Air flow rate (kg/s)	Total Pressure (Pa)	Efficiency (%)
Type 1	0.14	489.5	49.3
Type 2	0.14	562.7	58.1
Type 3	0.14	579.6	59.9
Type 4	0.14	555.1	58.3
Type 1	0.18	133.7	16.3
Type 2	0.18	250.2	33.9
Type 3	0.18	289.7	37.1
Type 4	0.18	247.7	33.1

Fig.22 shows Streamlines of fans using different diffusers at air flow rate of 0.14kg/s. There is no transition part at the outlet of the fan blade for Type 1 diffuser. A large amount of back flow appears near the fan outlet, leading to the flow loss. Type 2 and Type 4 diffusers avoid the appearance of the back flow. Thus, a suitable diffuser helps to increase fan's total pressure, efficiency, and maximum air flow rate. Although the fan using Type 3 diffuser has the higher total pressure and efficiency, it has a longer tail cone, which increases the overall size and weight of the fan. Considering the aerodynamic performance and practical application of the fan, it is more advantageous to choose Type 2 diffuser.

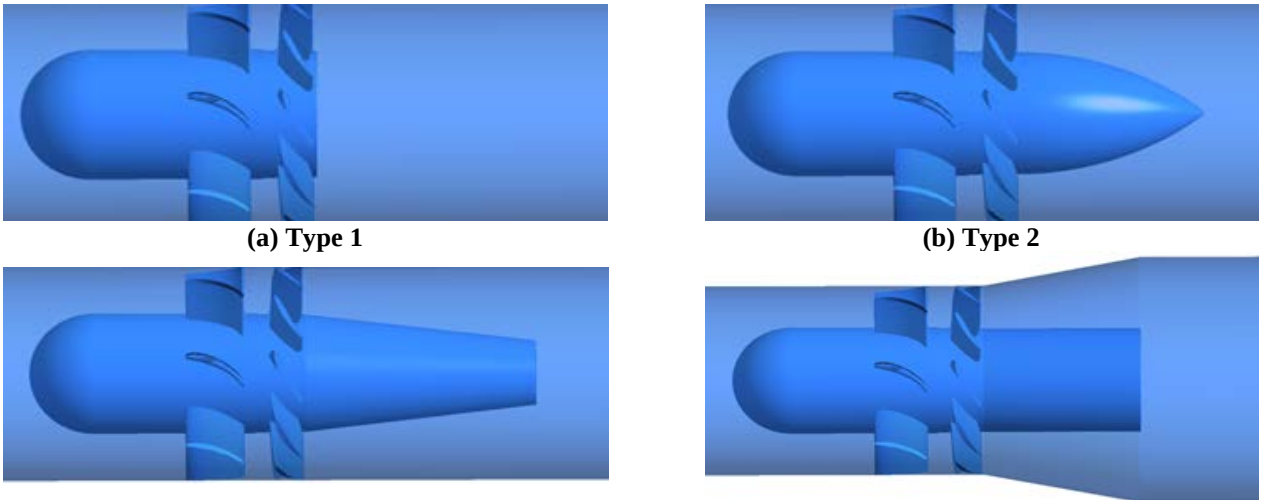

(a) Type 1 (b) Type 2

(c) Type 3 (d) Type 4

Fig.21 Schematics of fans using different diffusers

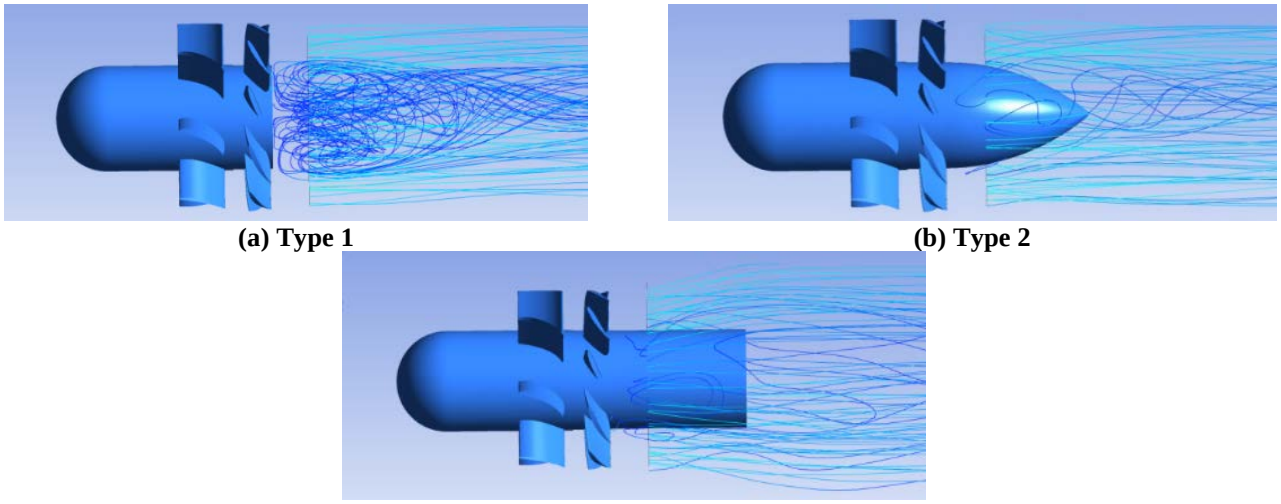

(a) Type 1 (b) Type 2

(c) Type 4

Fig.22 Streamlines of fans using different diffusers ($\dot{m} = 0.14kg/s$)

3.5 Influence of Front Guide Vanes

According to the operating conditions of the fan, it is sometimes necessary to install the guide vanes at the inlet or outlet of the fan. This section studies the effect of different numbers of front guide vanes on the performance of the fan. The fans with different number of front guide vanes are shown in Fig.23.

Table 3 shows the total pressure and efficiency of the fans with different numbers of front guide vanes. When the numbers of front guide vanes are 7, 9 and 15, the total pressures of the fans are increased by 86.1%, 76.1% and 12.5%, respectively, compared to that of the fan without front guide vane. However, only when the number of front guide vanes is 7, the efficiency of the fan is increased by 10%, and when the numbers of front guide vanes are 9 and 15, the efficiencies of the fans are reduced. Therefore, the front guide vanes can significantly increase the total pressure of the fan, but it is necessary to select a suitable number of front guide vanes because the excessive number of front vanes leads to a reduction in the efficiency of the fan.

Table 3 Influence of different numbers of front guide vanes on the performance of the fans (H=20km, $\dot{m} = 0.14kg/s$)

Numbers of Front Guide Vanes	Total Pressure (Pa)	Efficiency (%)
N_d=0	302.4	52.8
N_d=7	562.9	58.1
N_d=9	532.4	51.7
N_d=15	340.2	37.8

Fig.24 shows streamlines and pressure contours of the front guide vanes cross section airfoils at air flow rate of 0.14 kg/s. Because of the existence of the front guide vane, the gas is accelerated at the inlet of the fan blades and produces a certain deflection, changing AoA of the fan blades. However, at the same time, the flow loss is increased when the gas passes through the front guide vanes, and the pressure at the inlet of the front guide vanes is increased, which is disadvantageous in increasing the total pressure and efficiency of the fan. Therefore, a suitable number of front guide vanes can improve the performance of the fans at high altitude.

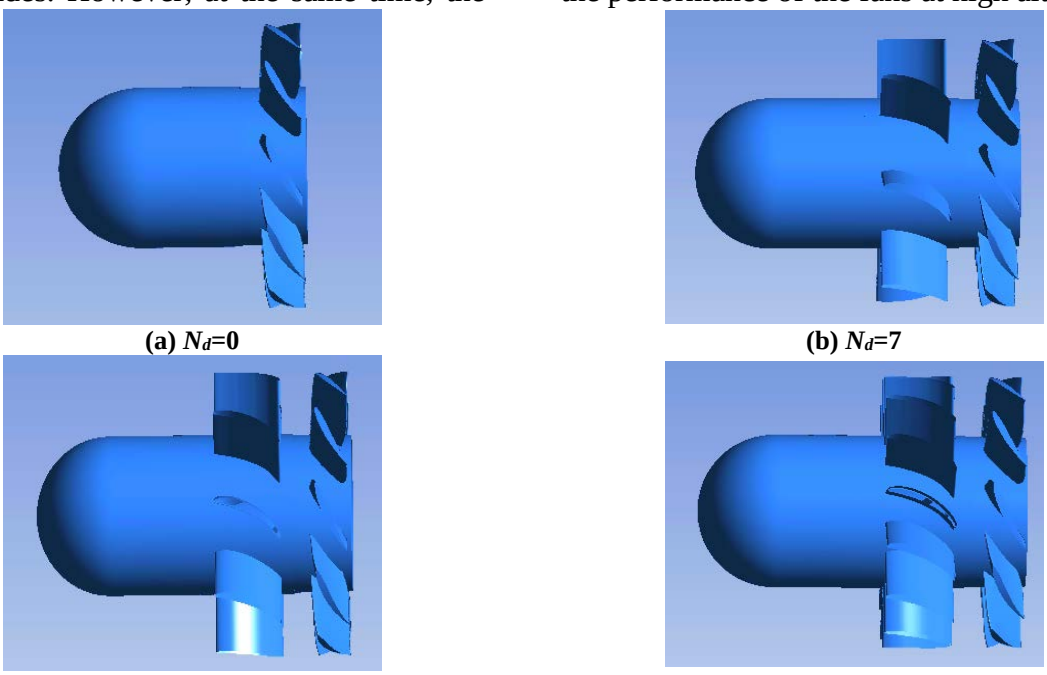

(a) N_d=0 **(b) N_d=7**

(c) N_d=9 **(d) N_d=15**

Fig.23 Schematics of fans using different front guide vanes

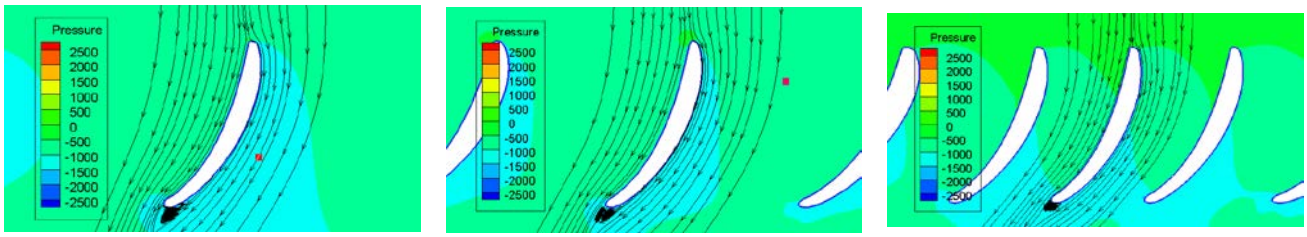

(a) N_d=7 **(b) N_d=9** **(c) N_d=15**

Fig.24 Streamlines and pressure contours of the front guide vanes cross section airfoils (r/R=0.5, $\dot{m} = 0.14kg/s$)

4 Conclusions

The flow field characteristics and the influence of key components of the large-discharge fan at 20km are researched deeply by numerically solving RANS equations. The conclusions obtained are as follows:

(1) The airfoil with high lift-drag ratio at low-Reynolds-number condition can increase the total pressure and efficiency of the fan, reduce the flow losses and increase the maximum air flow rate. The self-designed low-Reynolds-number PLRMS10 airfoil is one of the choices.

(2) The streamline current collector is a better choice to improve the overall aerodynamic performance of the large-discharge fan at high altitude.

(3) Considering the aerodynamic performance and practical application of the fan, the diffuser including the cylindrical wind tube and streamline tail cone should be used.

(4) The front guide vanes can significantly increase the total pressure of the fan, but the excessive number of front vanes has no advantage to the efficiency of the fan.

Acknowledgements

The research is funded by the National Natural Science Foundation of China (Grant No. 11272263).

References

[1] Muti Lin J. C., Pauley L. L. Low-Reynolds-Number Separation on an Airfoil. *AIAA Journal*, Vol. 34, No. 8, pp 1570-1576, 1996.

[2] Sunada S, Sakaguchi A, Kawachi K, et al. Airfoil Section Characteristics at a Low Reynolds Number. *Journal of Fluids Engineering*, Vol. 119, No, 1, pp 129-135,1997.

[3] McGhee R. J., Walker B.S. and Millard B. F. Experimental results for the Eppler 387 airfoil at low Reynolds numbers in the langley low-turbulence pressure tunnel. *NASA*, TM4062, 1988.

[4] Jones L. E. Numerical Studies of the Flow around an Airfoil at Low Reynolds Number. *Thesis for the degree of Doctor of Philosophy*, University of Southampton, 2008.

[5] Bohorquez F, Pines D. Hover Performance of Rotor Blades at Low Reynolds Numbers for Rotary Wing Micro Air Vehicles. *AIAA Journal*, 2013.

[6] Sunada S, Yasuda T, Yasuda K, et al. Comparison of Wing Characteristics at an Ultralow Reynolds Number. *Journal of Aircraft*, Vol. 39, No. 39, pp 331-338, 2015.

[7] Benni E. Three-dimensional multi-objective design optimization of a transonic compressor rotor. *Propulsion and power*, Vol. 20, No. 3, pp 559-565, 2004.

[8] Vad J., Kwedikha ARA., Horvath C., etc. Aerodynamic effects of forward blade skew in axial flow rotors of controlled vortex design. *Journal of Power and Energy*. Vol. 221, No. 7, pp 1001-1023, 2007.

[9] Seo S.J., Choi S.M., Kim K.Y. Design optimization of a low-speed fan blade with sweep and lean. *Journal of Power and Energy*, Vol. 222, pp 87-91, 2008.

[10] Louw F.G., Bruneau P.R.P., Backstrom T.W.V., etc. The design of an axial flow fan for application in large air-cooled heat exchangers. *Proceedings of ASME Turbo Expo*, Denmark, 2012.

[11] Menter F.R., Langtry R.B., Likki S.R., etc. A correlation-based transition model using local variables-part I: model formulation. *Journal of turbomachinery*, Vol. 128, pp 413-422, 2006.

[12] Langtry R.B., Menter F.R., Likki S.R., etc. A correlation-based transition model using local variables-part II: test cases and industrial applications. *Journal of turbomachinery*, Vol. 128, pp 423-434, 2006.

Contact Author Email Address

ShunLei Zhang: zhangslnwpu@163.com

Copyright Statement